Numerical simulations of molecular multiphoton excitation models

Benny Carmeli, Israel Schek, Abraham Nitzan, and Joshua Jortner

Department of Chemistry, Tel-Aviv University, Tel Aviv, Israel
(Received 20 March 1979; accepted 2 May 1979)

In this paper we report the results of numerical simulations of the intramolecular dynamics of a model system for multiphoton excitation of large molecules, where the low energy range is represented by a single discrete state, while the quasicontinuum is mimicked by two or three manifolds of molecular eigenstates. The random coupling model (RCM), where the radiative coupling matrix elements are assumed to be random functions of the level indices, yields conventional rate equations describing consecutive-reversible transitions for the populations with golden rule rates. In addition, numerical simulations were conducted for a constant coupling model (CCM) and for a separable random coupling model (SRCM), confirming the counterintuitive analytical results for these model systems. The time evolution of a RCM system is determined by the distribution function of the coupling elements and not by individual coupling terms, and the intramolecular dynamics is essentially determined by the lower moments (average and variance) of the distribution function. On the basis of numerical simulations we have shown that a radiative RCM, based on the molecular eigenstates, is equivalent to an intramolecular RCM founded on a zero-order molecular basis with a small number of optically active modes, random anharmonic coupling, and constant selective radiative interaction terms. Our computer experiments provide evidence for the validity of a strong coupling kinetic master equation for the RCM and suggest that random coupling is essential for the erosion of phase coherence effects in the multiphoton excitation of a molecular quasicontinuum.

I. INTRODUCTION

The theory of multiphoton excitation of "isolated" collision-free large molecules (see Fig. 1) is of considerable current interest. Experimental evidence[1] suggests that first-order kinetic equations for populations provide a good description of the collisionless multiphoton excitation processes in the quasicontinuum part (Region II) and in the continuous (Region III) part of the molecular vibrational manifold in large molecules, such as SF_6, while coherent effects underline the process within the few discrete bottom levels (Region I). Much effort has been devoted to deriving kinetic equations for the intramolecular dynamics of a molecule resulting from incoherent multiphoton excitation in Ranges II and III.[2-7] Recently, we have advanced a theory[2,3] for multiphoton excitation of large molecules which rests on the idea that the radiative coupling between the molecular vibrational–rotational eigenstates in Regions II and III are essentially random functions of the quantum numbers of the molecular eigenstates. This random coupling leads to erosion of coherence effects and results in a master equation for the time evolution of the probability distribution for the number of photons absorbed.

Alternative approaches to the problem of time evolution associated with multiphoton excitation of large molecules have been formulated by several workers.[4-7] These are based in one way or another on a picture in which coherence is lost due to a rapid intramolecular vibrational relaxation. This intramolecular vibrational relaxation in an isolated molecule involves essentially a dephasing process in the reduced space spanning the populations of the optically active mode(s) or, alternatively, in the reduced space spanning the number of photons absorbed. The rapid intramolecular dephasing limit is expressed by the inequality

$$\tau_{\mathrm{IVR}}^{-1} \gg \frac{|\bar{\mu}|}{\hbar} \tag{1a}$$

where τ_{IVR} is the time associated with the intramolecular vibrational energy redistribution and $\bar{\mu}$ is the scalar product between the electric field associated with the IR pulse and between the transition moment for IR ab-

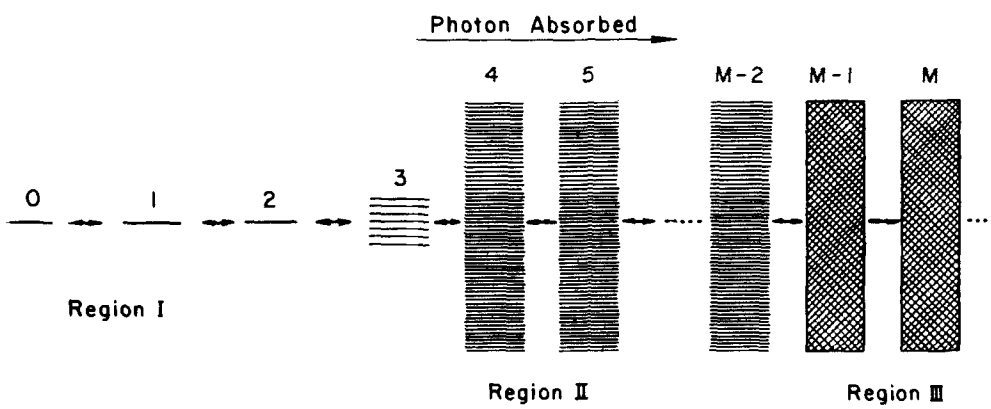

FIG. 1. A model for multiphoton excitation of a large molecule. Each manifold L corresponds to molecular levels (at different degrees of excitation) with a different number $(n-L)$ of photons. n is the initial number of photons and L denotes the number of photons absorbed.

 0021-9606/80/031928-10$01.00

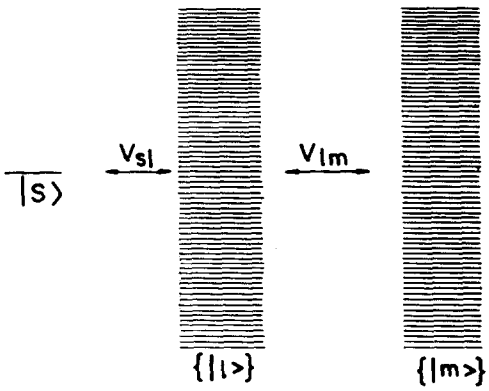

FIG. 2. A simplified multiphoton absorption model. Region I is represented by a single discrete level $|s\rangle$, while Regions II and III are represented by two manifolds $L \equiv \{|l\rangle\}$ and $M \equiv \{|m\rangle\}$.

sorption associated with the optically active molecular mode(s). The rhs of Eq. (1a) is the Rabi frequency, which characterizes the molecular IR excitation process. In the approach described in Refs. 2 and 3, Eq. (1a) is replaced by

$$(\Delta\omega)_{ab} \gg |\bar{\mu}| \ , \tag{1b}$$

where $(\Delta\omega)_{ab}$ is the energetic width of the IR absorption line shape of a molecule pre-excited into Regions II or III. Assumptions (1a) and (1b) are obviously identical since the width $(\Delta\omega)_{ab}$ is determined by the intramolecular relaxation process. However, there appears to be a conflict between theories in which condition (1) seems sufficient in order to obtain a simple Pauli master equation for the populations (or rather for the number of photons absorbed), and between the approach which invokes in addition the condition of random radiative coupling between molecular eigenstates.

Previous studies[8,9] indicate that the Markovian assumption (1) does not by itself lead to a simple master equation for the populations without additional assumptions concerning the nature of the radiative coupling. Let us consider a simplified model system for the multiphoton excitation process which incorporates all the physically relevant ingredients for the problem at hand. We shall simplify the conventional molecular model for multiphoton excitation (Fig. 1) by replacing Region I by a single discrete level $|s\rangle$ and Region II (and III) by two quasicontinua $\{|l\rangle\}$ and $\{|m\rangle\}$ (see Fig. 2). The radiative coupling elements are μ_{sl} and μ_{lm}. Assumption (1) allows us to disregard the systematic variations of μ_{sl} and μ_{lm} with the molecular level indices l and m. This still leaves us with the freedom to specify the nonsystematic variations of these matrix elements. The following models have been studied:

(a) *The random coupling model* (RCM),[2,3] where μ_{sl} and μ_{lm} are random functions of the indices l and m satisfying

$$\langle \mu_{sl} \rangle = \langle \mu_{lm} \rangle = 0 \ ,$$
$$\langle \mu_{sl}\mu_{sl'} \rangle = \langle \mu_{sl}^2 \rangle \delta_{ll'} \ ,$$
$$\langle \mu_{lm}\mu_{l'm'} \rangle = \langle \mu_{lm}^2 \rangle \delta_{ll'}\delta_{mm'} \ , \tag{2}$$

(b) *The asymmetric* RCM,[3] where

$$\mu = \langle \mu \rangle + \delta\mu \ , \tag{3}$$

with $\langle \mu \rangle \neq 0$ and where $\delta\mu$ rather than μ satisfies Eq. (2);

(c) *The separable* RCM[9]: the intercontinuum coupling μ_{lm} is separable as $\mu_{lm} = \mu_l \mu_m$. μ_{sl}, μ_l, and μ_m are random functions of l and m, satisfying

$$\langle \mu_{sl} \rangle = \langle \mu_l \rangle = \langle \mu_m \rangle = 0 \ ,$$
$$\langle \mu_l \mu_{l'} \rangle = \langle \mu_l^2 \rangle \delta_{ll'} \ ,$$
$$\langle \mu_m \mu_{m'} \rangle = \langle \mu_m^2 \rangle \delta_{mm'} \ ,$$
$$\langle \mu_{sl}\mu_{sl'} \rangle = \langle \mu_{sl}^2 \rangle \delta_{ll'} \ , \tag{4}$$

(d) *The constant coupling model* (CCM)[8]: μ_{sl} and μ_{lm} are constants independent of the indices l and m.

In view of the assumption (1b) that the molecular IR excitation linewidth in Regions II and III considerably exceed any other energy scale in the problem (i. e., the Rabi frequency, the inverse density of states, and the widths associated with the relaxation rates), we assume that the averaged quantities appearing in Eqs. (2)–(4) are constants independent of the state indices l and m. Note, however, that in the simulation models described below, the bandwidth $\Delta\omega$ appear naturally as the energy spread of the manifolds L and M.

All these four models lead to first-order Markovian kinetic equations for the population P_s, P_L, and P_M of the level s and the manifolds $L \equiv \{l\}$ and $M \equiv \{m\}$. These correspond to the probability of absorbing one or two photons. The kinetic equations for cases (a)–(d) may all be represented in the general form

$$\dot{P}_s = -(k_{s\to L} + k_{s\to M}) P_s \ ,$$
$$\dot{P}_L = -k_{L\to M} P_L + k_{M\to L} P_M + k_{s\to L} P_s \ ,$$
$$\dot{P}_M = -k_{M\to L} P_M + k_{L\to M} P_L + k_{s\to M} P_s \ . \tag{5}$$

The rates coefficients are different for the different models and are given in Table I. The RCM yields the "conventional" rate equation describing consecutive reversible transitions with golden rule rates. The separable RCM also leads to a consecutive rate process characterized by non-golden rule rates which are bounded by ρ_L^{-1}, the average level spacing in manifold L. Thus, the intercontinuum transition rates $k_{L\to M}$ and $k_{M\to L}$ are strongly damped in this case. In contrast to these cases, the CCM is characterized by a nonconsecutive time evolution in which the one-photon and the two-photon absorption processes occur simultaneously. The simultaneous rates $k_{s\to L}$ and $k_{s\to M}$ are retarded for the CCM; the retardation is appreciable in the strong intercontinuum coupling limit $N \gg 1$, where

$$N = \pi^2 |\mu_{lm}|^2 \rho_L \rho_M \ . \tag{6}$$

Finally, we note that the time evolution characterizing the asymmetric RCM is given as a superposition of the RCM and the CCM rates.

In view of the "counterintuitive" nature of the results for the CCM and for the separable RCM, it is apparent that Eq. (1) does not constitute a sufficient condition for the applicability of a "conventional" Pauli master equation for the populations. The derivation of the kinetic equations for the RCM rests on several assumptions. Schek and Jortner[2] have provided a plausibility argument

TABLE I. Rate constants.[a,b]

Model	CCM[8]	Random coupling models: Separable RCM[9] $\langle\mu\rangle=0$	RCM[2,3] $\langle\mu\rangle=0$	Asymmetric RCM[3] $\langle\mu\rangle\neq 0$
N	$\pi^2\mu_{lm}^2\rho_L\rho_M$	$\pi^2\langle(\mu_l\mu_m)^2\rangle\rho_L\rho_M$	0	$\pi^2\langle\mu_{lm}\rangle^2\rho_L\rho_M$
$k_{S\to L}$	$\frac{2\pi\mu_{sl}^2\rho_L}{(1+N)^2}$	$2\pi\langle\mu_{sl}^2\rangle\rho_L$	$2\pi\langle\mu_{sl}^2\rangle\rho_L$	$2\pi\langle\delta\mu_{sl}^2\rangle\rho_L+\frac{2\pi\langle\mu_{sl}\rangle^2\rho_L}{(1+N)^2}$
$k_{S\to M}$	$\frac{2\pi\mu_{sl}^2\rho_L\cdot N}{(1+N)^2}$	0	0	$\frac{2\pi\langle\mu_{sl}\rangle^2\rho_L\cdot N}{(1+N)^2}$
$k_{L\to M}$	0	$\frac{2N}{\pi\rho_L(1+N)^2}$	$2\pi\langle\mu_{lm}^2\rangle\rho_M$	$2\pi\langle\delta\mu_{lm}^2\rangle\rho_M$
$k_{M\to L}$	0	$\frac{1+N^2}{\pi\rho_L(1+N)^2}$	$2\pi\langle\mu_{lm}^2\rangle\rho_L$	$2\pi\langle\delta\mu_{lm}^2\rangle\rho_L$

[a]The molecular level structure involves the molecular eigenstates with radiative coupling between adjacent manifolds.

[b]ρ_L and ρ_M are density of levels in the L and M manifolds, respectively.

for the applicability of the RCM which essentially rests on the notion of diagonal singularity,[10] while Carmeli and Nitzan[3] have advanced a complete treatment using ensemble average methods and assuming a Gaussian distribution of the coupling terms. Furthermore, in contrast to weak coupling methods usually used to derive the Pauli master equation,[11] the RCM results in simple kinetic euqations under the conditions of strong coupling, i.e., $\langle\mu_{sl}^2\rangle^{1/2}\rho_l\gg 1$ and $N\gg 1$. As the characteristics of the RCM deserve further investigation, we have undertaken a numerical simulation study of a variety of different coupling schemes, all of which satisfy the restrictions posed by Eq. (2), in order to provide a numerical test for the results summarized in Table I.

Furthermore, these numerical simulations are useful in order to test some assumptions which underline the derivation of the results for the different coupling models and, in particular, the RCM. The details of the numerical simulation procedure are described in Sec. II. In Sec. III, we present some results of these simulations which strongly support the validity of the analytical results [Eq. (5) and Table I]. Finally, in Sec. IV, we explore the features of molecular models which provide some justification for the notion of random radiative coupling. Our results provide justification for the approximations and assumptions which underline the derivation of the kinetic equations for random coupling models for multiphoton excitation of large molecules.

II. THE SIMULATION PROCEDURE

Numerical calculations of multilevel coupling models have previously been carried out by several workers.[12-14] In particular, we mention the recent work by Quack,[15] who performed numerical calculations on intercontinuum coupling models for multiphoton excitation of large molecules. Quack's approach is based on random initial phases rather than on random coupling elements, so that the present study is in this sense complementary to his work.

In the present simulations, the quasicontinua L and M (Fig. 2) were represented by manifolds of (equally or randomly spaced) ~ 50–75 levels each. For the different random coupling cases, the coupling matrix elements were computer generated as random numbers with a prescribed distribution. Different coupling elements were assumed to be uncorrelated. The probability distribution for any given coupling element was taken to be one of the following three:

Gaussian:

$$P(\mu)=\sqrt{\frac{1}{2\pi\langle(\mu-\langle\mu\rangle)^2\rangle}}\exp\left[-\frac{(\mu-\langle\mu\rangle)^2}{2\langle(\mu-\langle\mu\rangle)^2\rangle}\right], \quad (7)$$

Uniform:

$$P(\mu)=\begin{cases} p=(b-a)^{-1}, & a\leq\mu\leq b, \\ 0, & \text{otherwise}, \end{cases} \quad (8)$$

Bimodal:

$$P(\mu)=\begin{cases} p_1 & \mu=a, \\ p_2=1-p_1, & \mu=b, \\ 0, & \text{otherwise}. \end{cases} \quad (9)$$

The values of the constants, p, p_1, a, and b in Eqs. (8) and (9) were chosen so that the values of $\langle\mu\rangle$ and of $\langle(\mu-\langle\mu\rangle)^2\rangle$ are identical for the different distributions.

With the set of coupling elements thus specified, we solve the time dependent Schrödinger equation by diagonalizing the Hamiltonian matrix and expressing the molecular wave functions as linear combinations of eigenfunctions of the molecule–radiation field Hamiltonian. We obtain the probabilities to populate the different quantum states as functions of time given that $P_s(t=0)=1$. Finally, we sum up the probabilities for all states belonging to a given manifold to obtain $P_s(t)$, $P_L(t)$, and $P_M(t)$. At all times, these three quantities should sum to unity, which provides a useful check on the numerical procedure. In most cases, we have performed an ensemble average of these probabilities, repeating the

calculation several times with a different set of initial random coupling elements. Typically, 10–15 "trajectories" were used for this average in order to obtain good statistics. The validity of the ensemble average procedure is discussed in Ref. 3(b). In some of the simulations described below, we demonstrate the applicability of this method.

The computer experiment described here suffers from inherent limitations dictated by the need to work with a relatively small number of states. Therefore, the dimensionless parameters $\langle \mu_{sl}^2 \rangle \rho_L^2$ and $\langle \mu_{lm}^2 \rangle \rho_M \rho_L$ are much smaller than in a typical real-life situation. Also, the manifolds L and M have a much smaller energetic spread in the simulation model than in most actual cases. However, for a time t which satisfies

$$(\Delta\omega_L)^{-1},\ (\Delta\omega_M)^{-1} \ll t/\hbar \ll \rho_L,\ \rho_M\ , \tag{10}$$

where $(\Delta\omega_L)$ and $(\Delta\omega_M)$ are the energy spread of the manifold L and M, respectively, we expect the manifolds L and M to behave as true continua of infinite extent. When $t/\hbar > \rho_L,\ \rho_M$, the numerical results will exhibit recurrences. When $t/\hbar \lesssim (\Delta\omega_L)^{-1},\ (\Delta\omega_M)^{-1}$, the uncertainty width of the levels is larger than the spread of the manifolds. In this initial time scale, the evolution is slow and may be represented by a Gaussian [$\exp(-t^2)$ for the decay of initial single level] rather than by an exponential function. When comparing the analytical results (obtained for large-spread continua) to the numerical simulations, we find that the simulation trajectory has shifted to somewhat longer times due to the slow initial evolution. In the results presented in the next section, we corrected this nonphysical effect by shifting the numerical result for the trajectory back to shorter times so that its initial evolution approximately coincides with the analytical result. A typical shift is of the order of 2% of the absolute time scale shown in the figures.

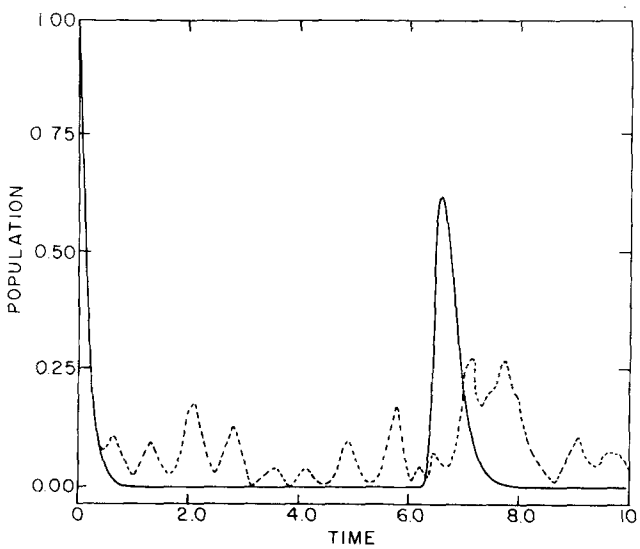

FIG. 3. Decay of a discrete level $|s\rangle$ into a manifold of 50 levels. $P_s(t)$ is the population of level $|s\rangle$. Level spacing is constant with $\rho = 3$. $\Gamma_s = 2\pi\langle\mu^2\rangle\ \rho = 6.28$. Full line: μ = constant; dashed line: μ = Gaussian random with $\langle\mu\rangle = 0$ (one trajectory).

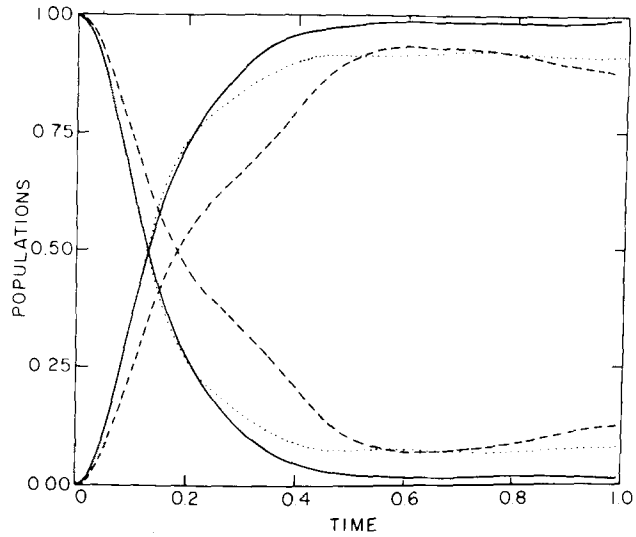

FIG. 4. Decay of a discrete level $|s\rangle$ into a manifold of levels. $\Gamma_s = 2\pi\langle\mu^2\rangle\ \rho = 6.28$. Gaussian random coupling with $\langle\mu\rangle = 0$. Full line: 150 levels, $\rho = 3$, single trajectory; dashed line: 50 levels, $\rho = 1$, single trajectory; dotted line: 50 levels $\rho = 1$, average over 15 trajectories.

As the interesting timescale is determined by the rates appearing in Table I, condition (10) implies that $\Delta\omega_L$ and $\Delta\omega_M$ should be taken much larger and that the level spacings ρ_L^{-1}, ρ_M^{-1} should be taken much smaller than these rates. If we identify the interesting time scale t with the golden rule rate so that $2\pi\langle\mu^2\rangle\ \rho t/\hbar \sim 1$, inequality (10) implies that two conditions should be satisfied. First, we require that $2\pi\langle\mu^2\rangle\ \rho \gg \rho^{-1}$, which results in the limit of strong intercontinuum coupling, i.e., $N \gg 1$. Second, we demand that $\Delta\omega \gg 2\pi\langle\mu^2\rangle\ \rho$. The choice of parameters $\Delta\omega$, $|\mu|$, and ρ for the simulation model should adhere to these restrictions.

In the presentation of all our numerical results, the unit of time is $\hbar$ and the unit of energy is 1.

III. NUMERICAL RESULTS FOR DYNAMICS OF COUPLED QUASICONTINUA

Figure 3 portrays the decay of a single discrete level into a manifold of 150 levels with level density $\rho = 3$, characterized by random and by constant coupling. We observe the exponential decay, the recurrence at long time for the case of constant coupling, and the Gaussian evolution at very short times. The random and the constant coupling models behave similarly within the range $t < \hbar\rho$ which is in accord with previous results.[12,13] For longer times, the CCM exhibits pronounced recurrences. As it is well known, the recurrence time $t_r = 2\pi\hbar\rho$ is valid only for the CCM. For the sample level structure of Fig. 3, the recurrence time is, in general, $t_r = 2\pi\hbar N_j/|E_j - E_s|$, where $\{E_j\}$ are the energies of the molecular eigenstates, while $\{N_j\}$ is a set of integers. Thus, for the RCM, $t_r = 2\pi\hbar/\Delta_j$, where Δ_j is the smallest common denominator of the energy spacings. To assess the effects of ensemble averaging, we have conducted further calculations for the same simple model with random coupling, which are displayed in Fig. 4. Here the result obtained for single trajectories (the two single tra-

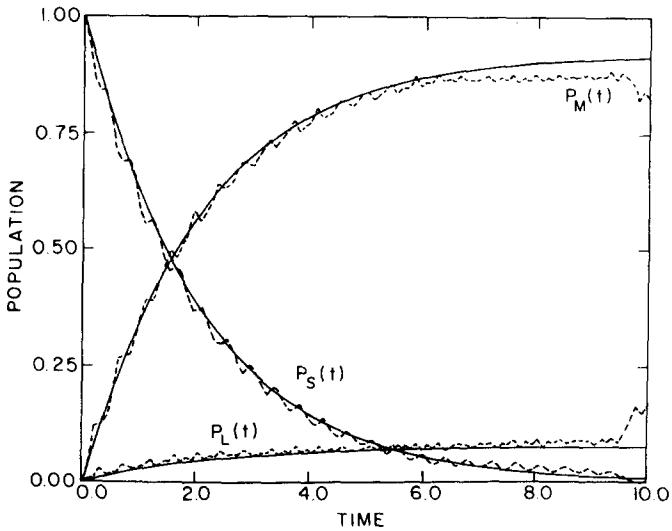

FIG. 5. Time evolution for the model of Fig. 2 with constant coupling. $\mu_{SL}=1$, $\mu_{LM}=0.9$, $\rho_L=1$, $\rho_M=1.5$. Full line: analytical result; dashed line: simulation for 50 levels in each of the L manifolds.

jectories are characterized by the same rates $2\pi\langle V^2\rangle\rho$ but different values of ρ) is compared to an ensemble average over 15 trajectories. It is seen that the ensemble average concept is reasonable; as ρ increases, the single trajectory result approaches that of the ensemble averaged one (the remaining difference in the asymptotic behavior results from the fact that for $\rho=3$ the dilution factor is three times larger; therefore, the asymptotic population of the state $|s\rangle$ is three times smaller than for $\rho=1$). Furthermore, different single trajectories calculated for the case with $\rho=3$ reproduced each other quite well on the timescale shown.

Figure 5 presents the time evolution of the model system of Fig. 2, which corresponds to the CCM, together with the analytical results from Table I. Figure 6 presents similar results for the separable RCM. Figures 7–9 compare the results of the numerical simulation with the analytical results for the symmetric RCM with Gaussian, uniform, and bimodal distributions, respectively, while Fig. 10 compares the simulation results corresponding to these three dimensions. Figure 11 displays simulation and analytical results for the asymmetric RCM.

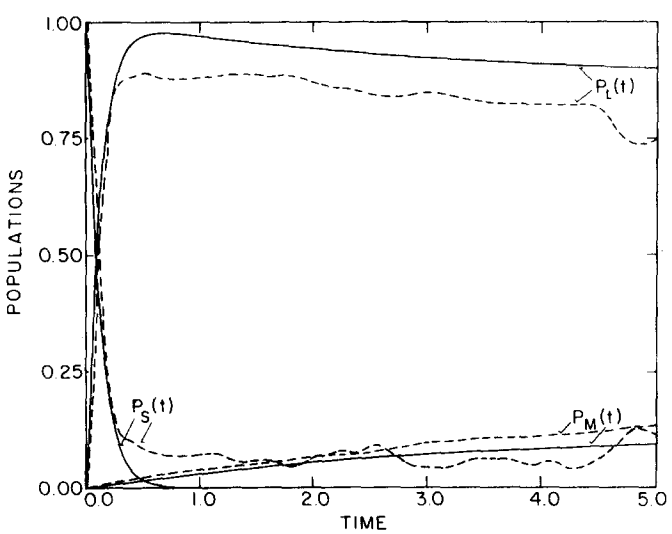

FIG. 6. Time evolution for the model of Fig. 2 with separable coupling. $\mu_{lm}=\mu_l\cdot\mu_m$, μ_{sl} μ_l, and μ_m are sampled from a uniform distribution with $|\mu_{sl}|\leq 1.95$, $|\mu_l|$, $|\mu_m|\leq 1.73$. This corresponds to $\sqrt{\langle\mu_{sl}^2\rangle}=1.13$ and $\sqrt{\langle\mu_{lm}^2\rangle}=1.00$. $\rho_L=1$, $\rho_M=1.5$. Full line: analytical results; dashed line: simulation with 75 levels in each of the L and M manifolds.

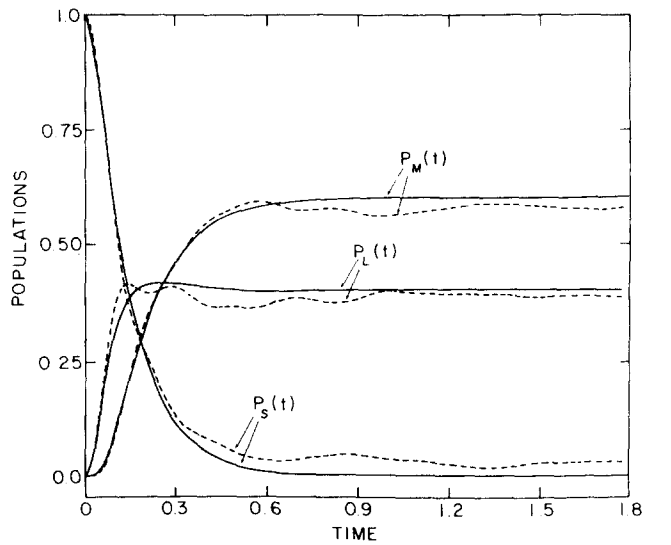

FIG. 7. Time evolution for the model of Fig. 2 with random coupling. μ_{sl} and μ_{lm} are sampled from a Gaussian distribution characterized by $\langle\mu_{sl}\rangle=\langle\mu_{lm}\rangle=0$ and $\sqrt{\langle\mu_{sl}^2\rangle}=1.13$, $\sqrt{\langle\mu_{lm}^2\rangle}=1.00$, $\rho_L=1.0$, $\rho_M=1.5$. Full line: analytical results; dashed line: simulation with 75 levels in each of the L and M manifolds.

In all the simulations on random coupling models, we used an ensemble average over 15 trajectories. As mentioned above, for large enough density of states, almost any single trajectory will coincide with the aver-

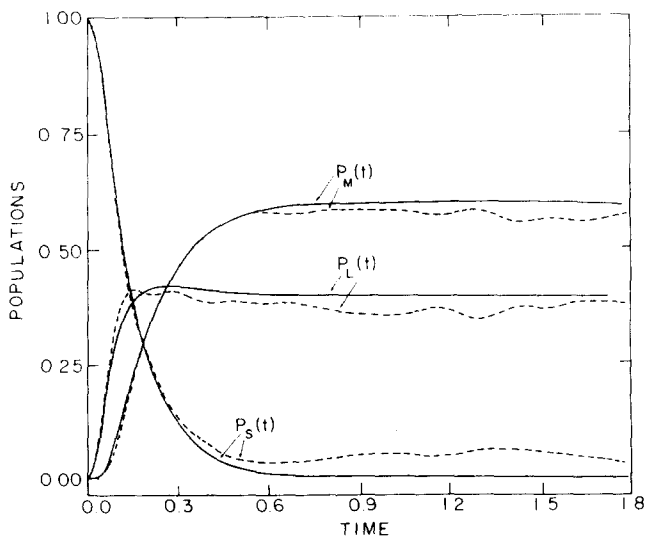

FIG. 8. Same as for Fig. 7 with μ_{sl} and μ_{lm} sampled from a uniform distribution $|\mu_{sl}|\leq 1.95$ and $|\mu_{lm}|\leq 1.73$ (corresponding to $\sqrt{\langle\mu_{sl}^2\rangle}$ and $\sqrt{\langle\mu_{lm}^2\rangle}$ as in Fig. 7).

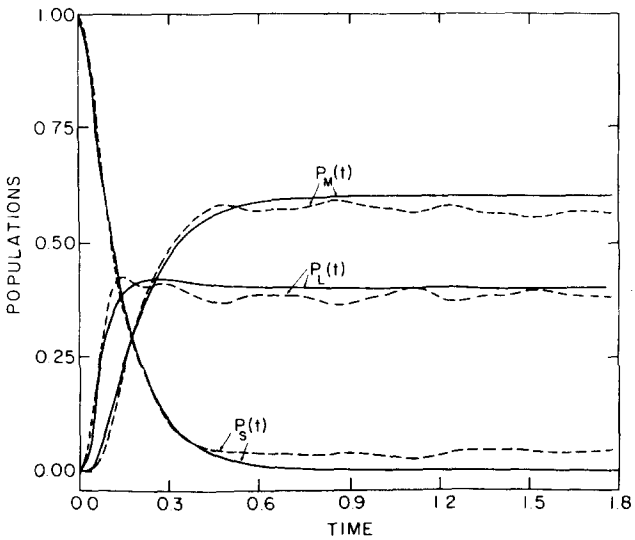

FIG. 9. Same as for Fig. 7 with a bimodal distribution $|\mu_{sl}| = \sqrt{1.13}$ and $|\mu_{lm}| = 1.0$ with random signs (corresponding to $\sqrt{\langle\mu_{sl}^2\rangle}$ and $\sqrt{\langle\mu_{lm}^2\rangle}$ as in Fig. 7).

aged one during short enough times ($t \ll \hbar\rho$) where the distribution of random coupling is reliably sampled over the levels within the uncertainty width $\hbar t^{-1}$. Figure 12 demonstrates this point again for the model of Fig. 2. In all simulations involving random coupling, taking the level spacing to be constant or to vary randomly with a given $\langle\rho\rangle$ was found to have little effect on the time evolution. The same is true also for constant coupling cases in the relevant $t < \hbar\rho$ time domain. Some further simulations and the corresponding analytical results for a single level coupled consecutively to three continua are displayed in Figs. 13 (for the CCM) and 14 (a Gaussian symmetric RCM). Here the statistics are worse than in the previous cases because a smaller number of levels are employed; however, the difference

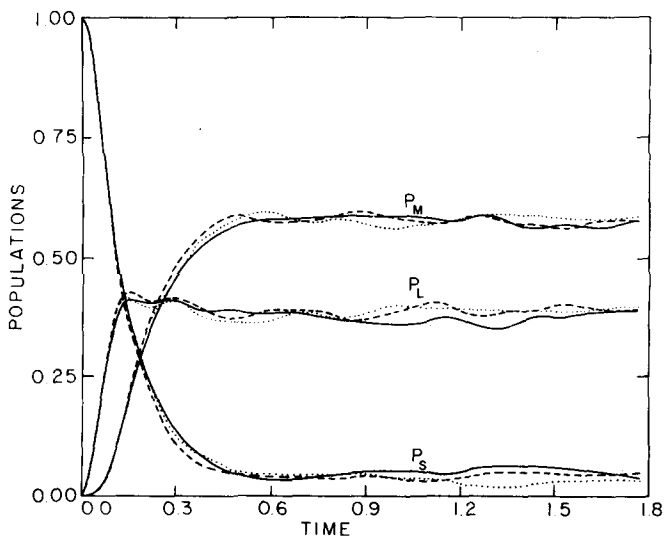

FIG. 10. A comparison of the simulation results displayed in Figs. 7–9 (Gaussian, uniform, and bimodal random coupling, respectively). Full line: uniform distribution; dashed line: bimodal distribution; dotted line: Gaussian distribution.

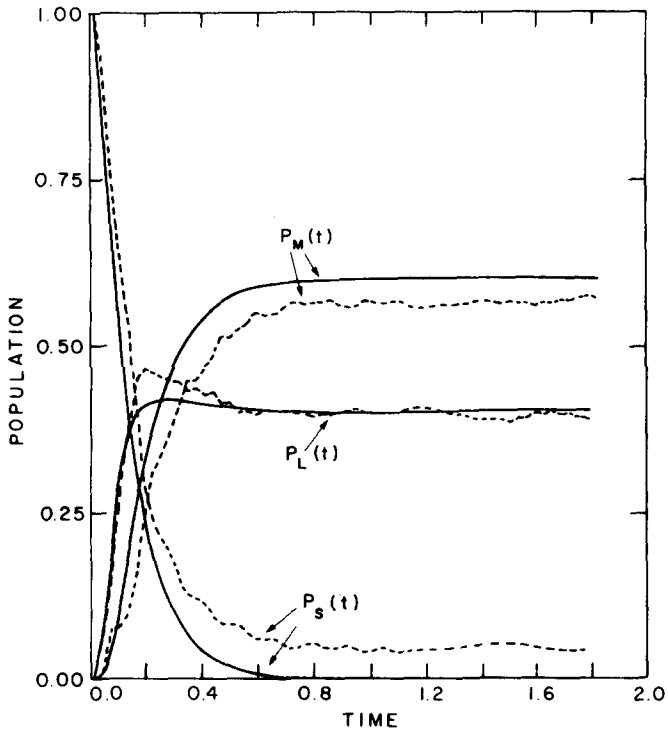

FIG. 11. Same as for Fig. 7 with an asymmetric Gaussian random coupling model. Parameters are identical to those of Fig. 7 only that $\langle\mu_{sl}\rangle = 1.0$ and $\langle\mu_{lm}\rangle = 0.9$.

between the CCM and the RCM behavior is clearly visible.

From the results of these computer experiments, we conclude the following:

(A) The analytical results for all the four coupling

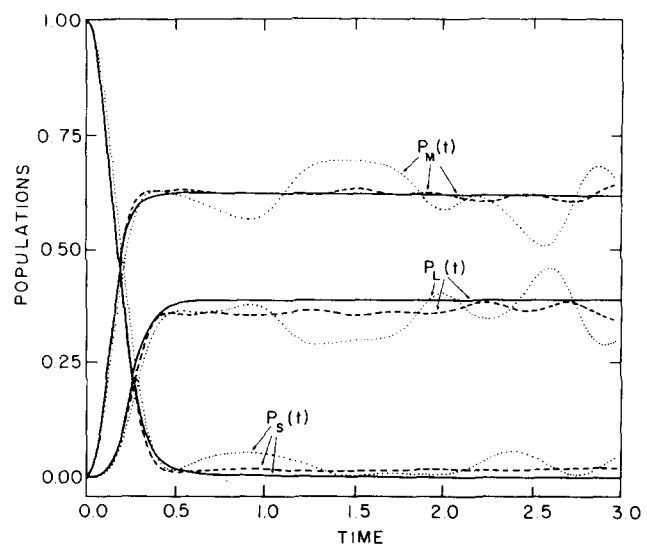

FIG. 12. Comparison of a single time evolution trajectory and an average over 15 trajectories for the model represented in Fig. 2 with Gaussian random coupling characterized by $\langle\mu_{sl}\rangle = \langle\mu_{lm}\rangle = 0$, $\sqrt{\langle\mu_{sl}^2\rangle}$, $\sqrt{\langle\mu_{lm}^2\rangle} = 0.6$. $\rho_L = 8$, $\rho_M = 5$. Full line: analytical results ($k_{S\to L} = 12.6$, $k_{L\to M} = 11.3$, $k_{M\to L} = 18.1$); dashed line: simulation with 90 levels in the L and 59 levels in the M manifolds, averaged over 15 trajectories; dotted line: a typical single trajectory.

models of Table I are confirmed. We were thus able to provide a justification for assumptions and approximations which underline the derivations of all these results. In particular, the results of the numerical simulations provide a clear demonstration for the validity of the RCM which plays a central role in our theory of multiphoton excitation of large molecules.[2,3]

(B) The time evolution of a system characterized by a random distribution of coupling matrix elements is determined only by the distribution function of these elements and not by the exact values of the different coupling terms. This assumption implies that ensemble average methods are applicable.

(C) The time evolution in a system characterized by random coupling is determined by the lower moments (average and variance) of the probability distribution for the coupling elements. The results presented in Table I for the RCM and separable RCM were derived by Carmeli and Nitzan[3] assuming Gaussian distribution of coupling elements. The assumption of Gaussian randomness does not impose a stringent restriction on the applicability of the analytical solution.

(D) The satisfactory agreement achieved between the results of the numerical simulations and the analytical results of Table I was accomplished for systems on the verge of the strong coupling situation with $\pi\langle\mu^2\rangle^{1/2}\rho \gg 1$. It should be emphasized that the conceptual basis for the RCM master equation, which rests on the strong coupling limit, is different from the conventional derivations of master equations[11] that invoke a weak coupling assumption. The latter, therefore, are not applicable to the problem of multiphoton excitation of a large molecule.

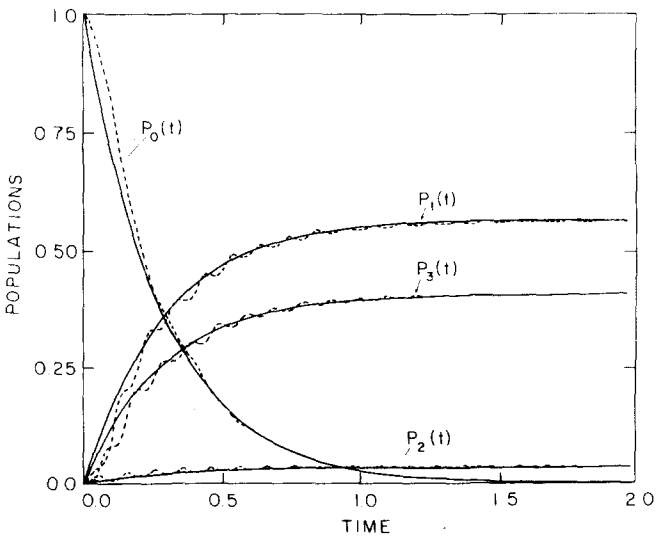

FIG. 13. Time evolution for a model composed of a single level $|0\rangle$ and three manifolds $1\equiv\{|1_j\rangle\}$, $2\equiv\{|2_j\rangle\}$, and $3\equiv\{|3_j\rangle\}$. $\rho_1=1.0$, $\rho_2=1.25$, $\rho_3=1.5$. Constant coupling: $\mu_{01}=1.0$, $\mu_{12}=0.9$, and $\mu_{23}=0.8$; full line: analytical results; dashed line: simulations with 40, 50, and 59 in manifolds 1, 2, and 3, respectively.

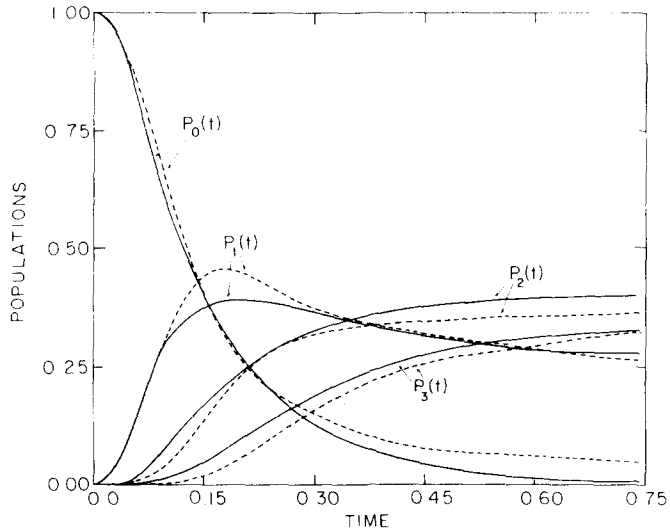

FIG. 14. Same as for Fig. 13. $\rho_1=1.0$, $\rho_2=1.25$, and $\rho_3=1.5$. Gaussian coupling random: $\sqrt{\langle\mu_{01}^2\rangle}=1.0$, $\sqrt{\langle\mu_{12}^2\rangle}=0.9$, and $\sqrt{\langle\mu_{23}^2\rangle}=0.8$; full line: analytical results; dashed line: simulations with 40, 59, and 50 levels in manifolds 1, 2, and 3, respectively.

IV. RANDOM COUPLING MODELS WITH ZERO-ORDER MOLECULAR STATES

The RCM for multiphoton excitation of isolated large molecules[2,3] rests on the notion of random radiative coupling between the molecular eigenstates, evading the issue of intramolecular vibrational energy redistribution. The results of the numerical simulations presented in Sec. III provide "experimental" evidence that random radiative coupling results in the total erosion of phase coherence effects. In our treatment, the Markovian condition (1) enters implicitly, providing a necessary but not a sufficient condition for the validity of a Pauli-type master equation for the populations. It is interesting to establish the relation between the picture based on radiative RCM, between molecular eigenstates, and an alternative approach which starts from a zero-order molecular basis and considers radiative coupling between a small number of zero-order modes, which in turn are coupled to the rest of the vibrational degrees of freedom.

The optically active zero-order states can be taken to be either harmonic normal modes or as bond modes. Both experimental and theoretical evidence is currently available indicating that for X–H bonds in aromatic and altiphatic hydrocarbons and in water the segregation of zero-order bond modes is physically acceptable.[16] Recent experimental evidence based on IR absorption and emission spectroscopy of a highly vibrationally excited SF_6 molecule provides strong support to the notion that in this system the zero-order ν_3 normal mode retains its identity up to relatively high energies, i.e., ~8000 cm^{-1} above the ground state.[4,17] The absorption spectra corresponding to transitions between states corresponding to the ν_3 zero-order normal mode at high energies are considerably broadened,[4,17] the typical widths being $\tilde{\Gamma}(W)\sim 10$–100 cm^{-1}, which provide an upper limit for

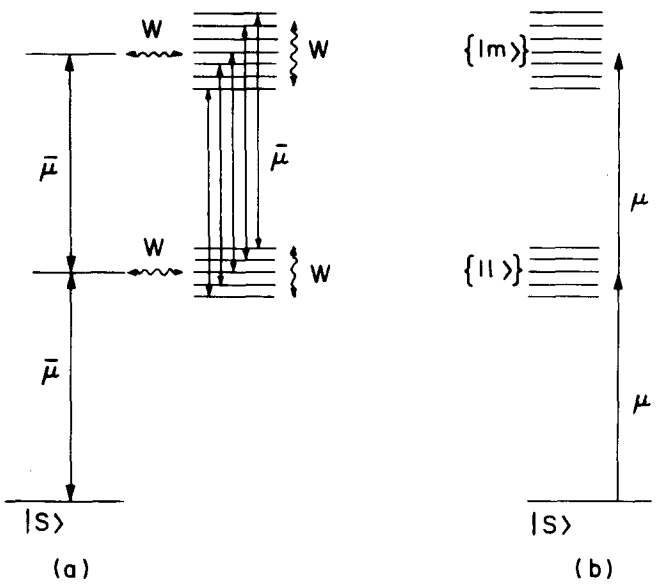

FIG. 15. A comparison between two molecular models. (a) Zero-order molecular levels with a single optically active mode and with unharmonic interactions; (b) Exact molecular eigenstates with diluted random radiative couplings.

the rate of intramolecular vibrational energy redistribution.

In Fig. 15, we compare the two complementary models for the description of multiphoton excitation in Regions II and III. Figure 15(a) portrays the intramolecular and the radiative coupling scheme in the zero-order molecular basis set in the simple case where a single mode is optically active. Consider first the radiative coupling. At each level of excitation, vibrational states are selectively radiatively coupled to states located at the higher level. Thus, each zero-order state is radiatively coupled to a single higher zero-order state, which corresponds to a change of one quantum in the optically active mode with no change in the other modes. The radiative coupling matrix elements $\bar{\mu}$, appearing in Fig. 15(a), correspond to the scalar product between the electric field and the dipole matrix elements which connect (zero-order) states corresponding to the optically active modes. The $\bar{\mu}$ terms are therefore weakly dependent of the level indices and can be taken as constant for each two consecutive manifolds.

Second, we consider the intramolecular coupling. At each level of excitation, the zero-order molecular states are coupled by an intramolecular perturbation W which corresponds to the anharmonicity and to off-diagonal kinetic energy contributions. The coupling W induces the intramolecular vibrational relaxation (or intramolecular dephasing). The characteristic time for the latter process is[16]

$$\tau_{\mathrm{IVR}} = \hbar/\Gamma^{(W)} \ , \tag{11}$$

where

$$\Gamma^{(W)} \equiv 2\pi\langle W^2\rangle\rho \tag{12}$$

is the associated width. Obviously, $\Gamma^{(W)} \simeq \Delta\omega_{\mathrm{AB}}$, which was defined in Eq. (1). The intramolecular coupling terms W_{ij} connecting zero-order states i and j involve (in Regions II and III) highly oscillatory vibrational wave functions. Thus, it is reasonable to assume that the intramolecular coupling terms involve random functions of the zero-order level indices i and j. A random coupling model for intramolecular vibrational energy redistribution was previously considered by several groups.[16(b),18-20] We thus assert that the multiphoton excitation model, which rests on the zero-order molecular basis [Fig. 15(a)], involves random intramolecular coupling and approximately constant radiative coupling.

On the other hand, the approach advanced in our previous work[2,3] and in Sec. III of the present paper considers random radiative coupling between those molecular eigenstates, which result from the diagonalization of the total molecular Hamiltonian (including the interaction W). The manifolds $\{|l\rangle\}$ and $\{|m\rangle\}$ [Fig. 15(b)] constitute linear combinations of the zero-order states appearing in Fig. 15(a). The consequences of the transformation between the zero-order basis and the molecular eigenstates basis regarding the latter are as follows: (a) The intramanifold intramolecular coupling W no longer appears, and only radiative coupling prevails. (b) The radiative coupling between adjacent manifolds of molecular eigenstates involves nonselective coupling. (c) This radiative coupling terms μ can be taken as random function of the level indices. (d) Conservation of integrated absorption intensities implies that level scrambling results in the "dilution" of the (constant) radiative coupling terms $\bar{\mu}$, which combine zero-order molecular eigenstates. We expect that in general $\mu \ll \bar{\mu}$. To derive the relation between the radiative coupling terms in both representations, one has to introduce the dilution factor for intramolecular coupling[3(c)]

$$D^{(W)} = \pi^2\langle W^2\rangle\rho^2 = \pi\Gamma^{(W)}\rho/2 \ . \tag{13}$$

The dilution is exhibited for $\bar{\mu}^2$ so that[3(b)]

$$\langle\mu^2\rangle \simeq \bar{\mu}^2/D^{(W)} \ . \tag{14}$$

Thus, the relation between the (properly averaged) Rabi frequency when the random radiative coupling prevails in the molecular eigenstates basis and between the (practically constant) Rabi frequency associated with an optically active mode in the zero-order molecular basis is

$$\langle\mu^2\rangle^{1/2} \simeq |\bar{\mu}|/(\pi\Gamma^{(W)}\rho/2)^{1/2} \ . \tag{14a}$$

It should be borne in mind that the random radiative coupling elements μ_{sl} and μ_{lm} used in the simulations of Sec. III are approximately determined by the "diluted" spread (variance) $\langle\mu^2\rangle$, which is given by Eq. (14).

To establish the relation between the conventional radiative RCM of Sec. III [see Fig. 15(b)] and the intramolecular RCM with constant radiative coupling between zero-molecular states [See Fig. 15(a)], we have performed some numerical simulations. In the computer experiments, we took all the $|\bar{\mu}|$ terms to be constant, corresponding to selective radiative coupling, while W was chosen to be random (with $\langle W\rangle = 0$), and $\Gamma^{(W)}$ was determined from Eq. (12). $\langle\mu^2\rangle$ was then calculated from Eq. (14). The diluted radiative coupling terms μ_{sl} and μ_{lm} were subsequently determined for the radia-

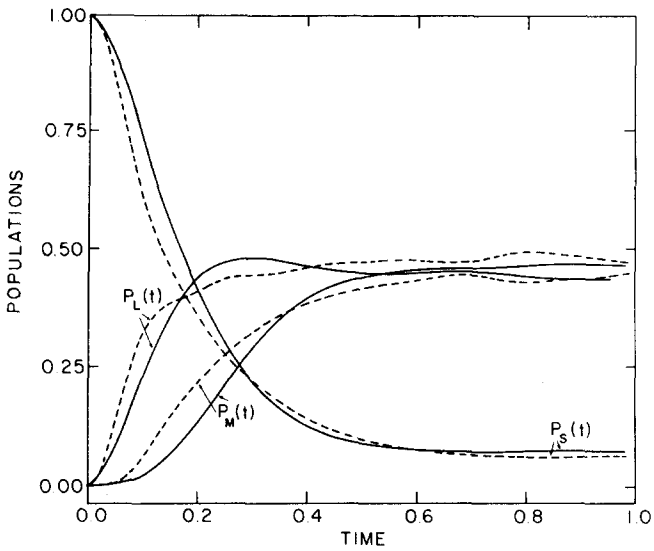

FIG. 16. Time evolution for the models described in Fig. 15. $P_s(t=0)=1$ in all cases. Each manifold is made from 70 levels with $\rho=1$. Full line: Evolution based on the coupling scheme from Fig. 15(a); $\bar{\mu}$ is taken the same way between all levels equal to $\sqrt{30}$; W is taken to be Gaussian random with $\langle W\rangle=0$ and $\langle W^2\rangle=3.0$; dashed line: evolution based on the coupling scheme from Fig. 15(b); μ is the Gaussian random with $\langle\mu\rangle=0$ and $\langle\mu^2\rangle=1.0$.

tive RCM taking $\langle\mu\rangle=0$. The relevant parameters were so chosen that $\Gamma^{(W)}>|\bar{\mu}|$, which is in accord with Eq. (1). In Fig. 16, we confront the time evolution for the two models. The agreement between the time evolution in the two models demonstrates the following:

(1) The dynamics of a system described by an intramolecular RCM with constant radiative coupling [Fig. 15(a)] results in a time evolution which is quite similar to the result obtained for the radiative RCM [Fig. 15(b)]. The small difference between the two evolution pathways displayed in Fig. 16 results from the approximation involved in Eq. (14).

(2) The time evolution of a system where random coupling prevails is essentially determined by the lower moments of the distribution function of the relevant (radiative or intramolecular) coupling elements.

(3) The "coarse graining" argument utilized in the derivation of the dilution effect (14) is justified.

(4) The master equation was obtained from simulations on a model system described by intramolecular RCM and constant radiative coupling [Fig. 15(a)] provided that $\Gamma^{(W)}>|\bar{\mu}|$, which is in accord with Eq. (1). This result is useful as it explicitly demonstrates the equivalence between our[2,3] necessary condition for the applicability of the master equation and alternative approaches[4-7] to the problem of multiphoton excitation of large molecules.

V. CONCLUDING REMARKS

We have demonstrated that both random radiative coupling between molecular eigenstates or, alternatively, random intramolecular coupling between zero-order states in the molecular quasicontinuum is essential in eroding the effects of phase coherence in the multiphoton excitation of a large molecule. The equivalence between the radiative RCM [Fig. 15(a)] and the intramolecular RCM [Fig. 15(b)] provides strong support for the validity of our physical approach[2,3] and for the description of collisionless multiphoton excitation of large molecules. Our results demonstrate that the simple kinetic Pauli master equation is valid for the description of multiphoton excitation of a molecular quasicontinuum provided that two conditions are simultaneously satisfied:

(1) rapid intramolecular dephasing [Eq. (1)],

(2) random coupling prevails.

We would like to conclude this discussion with several comments. First, our approach[2,3] for multiphoton excitation of a quasicontinuum, which rests on assumptions (1) and (2), differs from alternative theoretical approaches[4-7] which invoked just assumption (1). The physical condition for rapid intramolecular dephasing [Eq. (1)] provides a necessary, but not a sufficient, condition for the validity of the kinetic Pauli master equation for the multiphoton excitation of a congested molecular level structure. Second, we have provided evidence for the applicability of a master equation which corresponds to a strong coupling random coupling situation. Third, we have demonstrated that random coupling in collisionless multiphoton excitation can be taken to involve either intramolecular or radiative interactions, depending on the choice of the molecular basis. As long as off-resonance intramolecular interactions between zero-order molecular modes are small, the choice of the molecular basis set (in terms of molecular eigenstates or as zero-order states) is merely a matter of convenience.[16(b)] Fourth, we would like to draw attention to the breakdown of the Pauli master equation when the RCM applies but the Markovian condition (1) is no longer obeyed. In that case, the approach of Sec. IV, which rests on intramolecular RCM involving zero-order molecular states, will be useful for the understanding of coherent effects at extremely high fields, which will be exhibited in the excitation of a congested molecular level structure.

ACKNOWLEDGMENTS

B. C. and A. N. acknowledge the support of the Commission of Basic Research of the Israel Academy of Science and of the United States-Israel Binational Science Foundation, Jerusalem, Israel.

[1](a) P. Kolodner, C. Winterfeld, and E. Yablonovitch, Opt. Commun. 20, 119 (1977); (b) J. G. Black, E. Yablonovitch, N. Bloembergen, and S. Mukamel, Phys. Rev. Lett. 38, 113 (1977); (c) E. R. Grant, P. A. Schulz, A. S. Sadbo, Y. R. Shen, and Y. T. Lee, Phys. Rev. Lett. 40, 115 (1978).

[2]I. Schek and J. Jortner, J. Chem. Phys. 70, 3016 (1979).

[3](a) B. Carmeli and A. Nitzan, "Kinetic equations for multiphoton dissociation of large molecules," Chem. Phys. Lett. (in press); (b) B. Carmeli and A. Nitzan, "Random coupling

models for intramolecular dynamics. I. Mathematical approach," J. Chem. Phys. (in press); (c) B. Carmeli and A. Nitzan, "Random coupling models for intramolecular dynamics. II. Kinetic equations for collisionless multiphoton dissociation of large molecules," J. Chem. Phys. (in press).
[4]N. Bloembergen and E. Yablonovitch, Phys. Today **31**, 23 (1978).
[5]D. P. Hodgkinson and J. S. Briggs, J. Phys. B **10**, 2583 (1977).
[6]S. Mukamel, J. Chem. Phys. **70**, 2479 (1979).
[7]C. D. Cantrell, S. M. Freund, and J. L. Lyman, in *Laser Handbook* (North-Holland, Amsterdam, 1978), Vol. III(b).
[8](a) A. Nitzan, J. Jortner, and B. J. Berne, Mol. Phys. **26**, 281 (1973); (b) S. Mukamel and J. Jortner, Mol. Phys. **27**, 1543 (1974).
[9]B. Carmeli and A. Nitzan, Chem. Phys. Lett. **58**, 310 (1978).
[10]L. Van Hove, Physica (Utrecht) **21**, 517 (1955).
[11]R. Zwanzig, Physica (Utrecht) **30**, 110 (1964).
[12]W. M. Gelbart, D. F. Heller, and M. L. Elert, Chem. Phys. **7**, 116 (1975).
[13]J. M. Delory and C. Tric, Chem. Phys. **3**, 54 (1974).
[14]C. A. Langhoff and G. W. Robinson, Mol. Phys. **26**, 249 (1973).
[15]M. Quack, J. Chem. Phys. **63**, 1282 (1978).
[16](a) D. Heller and S. Mukamel, J. Chem. Phys. **70**, 463 (1979); (b) M. Sage and J. Jortner, "Resonance structure and background absorption in high overtone molecular spectra," Chem. Phys. Lett. **62**, 451 (1979).
[17]J. L. Lyman, R. V. Jensen, J. Rink, C. P. Robinson, and S. D. Rockwood, Appl. Phys. Lett. **27**, 87 (1975).
[18]C. Tric, Chem. Phys. **14**, 189 (1976).
[19]K. G. Kay, J. Chem. Phys. **61**, 5205 (1974).
[20]W. M. Gelbart, S. A. Rice, and K. F. Freed, J. Chem. Phys. **57**, 4699 (1972).